THREE PHASE EULERIAN-GRANULAR MODEL APPLIED ON NUMERICAL SIMULATION OF NON-CONVENTIONAL LIQUID FUELS COMBUSTION IN A BUBBLING FLUIDIZED BED

by

Stevan Dj. NEMODA*, Milica R. MLADENOVIĆ, Milijana J. PAPRIKA, Aleksandar M. ERIĆ, and Borislav D. GRUBOR

Laboratory for Thermal Engineering and Energy, Vinca Institute of Nuclear Sciences, University of Belgrade, Belgrade, Serbia

Original scientific paper
DOI: 10.2298/TSCI151025196N

The paper presents a 2-D CFD model of liquid fuel combustion in bubbling fluidized bed. The numerical procedure is based on the two-fluid Euler-Euler approach, where the velocity field of the gas and particles are modeled in analogy to the kinetic gas theory. The model is taking into account also the third – liquid phase, as well as its interaction with the solid and gas phase. The proposed numerical model comprise energy equations for all three phases, as well as the transport equations of chemical components with source terms originated from the component conversion. In the frame of the proposed model, user sub-models were developed for heterogenic fluidized bed combustion of liquid fuels, with or without water. The results of the calculation were compared with experiments on a pilot-facility (power up to 100 kW), combusting, among other fuels, oil. The temperature profiles along the combustion chamber were compared for the two basic cases: combustion with or without water. On the basis of numerical experiments, influence of the fluid-dynamic characteristics of the fluidized bed on the combustion efficiency was analyzed, as well as the influence of the fuel characteristics (reactivity, water content) on the intensive combustion zone.

Key words: *CFD model, combustion, fluidized bed, granular flow, liquid fuel, three-phase model*

Introduction

Gas-solid bubbling fluidized bed (BFB) reactors can be extensively used for various applications, such as gasification, catalytic processes, drying, combustion, and incineration. This technology is very attractive because it can be applied to the combustion of low quality coals, biomass, sewage sludge, and waste materials. Lately these reactors are repeatedly used for purposes of thermal disintegration (incineration) of industrial waste and by-products, with utilization of generated energy. Because of its high thermal inertia (thermal capacity), high thermal conductivity and very good mixing, an intensive heat transfer is characteristic for fluidized bed (FB). Due to a relatively low combustion temperature (between approximately 800 °C and 950 °C), the level of thermal NO_x in FB boilers is considerably reduced compared to most conventional boilers. This reduction is accomplished without the introduction of complex burners or additional flue gas treatment facilities. The efficient in-situ SO_2 removal is also an important aspect of emission control in FB boilers.

* Corresponding author; e-mail: snemoda@vinca.rs

For the purpose of developing incineration FB facilities, experimental methods and numerical simulations are lately equally employed. The CFD models provide great opportunities for saving resources and time in development of facilities and technologies in the fields of energy and process engineering. However, the numerical tools for simulation of complex processes such as BFB combustion – where it is necessary to simulate complex fluidized granular two phase flow, including the third phase of liquid or solid fuels and homogeneous/heterogeneous chemical reactions, are not completely developed. In addition, it is preferred that the numerical tool is also suitable to engineering needs, meaning it should not require large computational resources and long time.

Two approaches are frequently used for CFD modeling of gas-solid FB: the Euler--Lagrange (EL) approach and the Euler-Euler (EE) approach. In the EL approach [1, 2], the gas phase is treated as a continuous phase and modeled using an Eulerian framework, whereas the solid phase is treated as discrete particles, and described by Newton's laws of motion on a single particle scale, discrete particle modeling [3-5]. The advantage of the EL approach is that it allows studying the individual particle motion and particle-particle interactions directly, but this model requires powerful computational resources in large systems of particles, what is case of FB. In the EE approach [6-10], both the gas and solid phases are considered as fluids and as fully inter-penetrating continua. Both phases are described by separate conservation equations for mass and momentum. The EE approach is not limited by the particle number, and becomes a more natural choice for hydrodynamic modeling of engineering scale systems [11, 12]. However, additional closure equations are required in the EE approach to describe the stochastic motion and interaction of the solid phase. The kinetic theory of granular flow (KTGF) is commonly used to obtain constitutive relations for the solid phase. Particles in gas-solid flow may be treated as magnified molecules, and the analogy of their behavior to the gas molecules is the reason for wide use of the KTGF for modeling the motion of particles. This theory is basically an extension of the classical kinetic theory of non-uniform gases [13] to dense particulate flows. The KTGF is based on the concept of granular temperature, what is the measure of random oscillations of the particles and is defined as the average of the three variances of the particle's velocities.

Within the framework of the EE approach, applying a proper drag model is very important, where it should be taken into account that, in spite of detailed mathematical modeling of the complex processes in FB, the drag laws used in two-fluid models are semi-empirical in nature. The inter-phase interaction drag force model [14] is used often. In that model, the coefficient between fluid and solid (granular) phase depends only on the phase void fraction and the terminal velocity coefficient, but not on the minimum fluidization conditions. Therefore, correction constants in the expression for the terminal velocity coefficient should be performed, which is particularly important in the case of fluidization with chemical reactions [15, 16].

In this paper, the EE approach, also called granular flow model (GFM), has been chosen to simulate the combustion of an unconventional liquid fuel in a 2-D BFB reactor. The unconventional fuel is a combustible industrial liquid waste with significant water content. Within GFM calculation, the third phase has also been included in the process, which corresponds to a liquid fuel that is fed into the FB. The proposed numerical procedure also contains energy equations for all three phases, as well as the transport equations of chemical components with source terms due to the conversion of chemical species. Special attention is devoted to modeling the process of the liquid fuel combustion in the BFB. In addition to homogeneous reactions of gaseous components, heterogeneous reactions with evaporation and direct combustion of liquid fuel were taken into account.

For solving the system transport equations of the proposed EE model for liquid fuel combustion in BFB the software package FLUENT 14.0 was used. Thereby, for the models for the drag force, liquid fuel devolatilization and water evaporation, particular subroutines have been in-house developed.

The proposed EE model for liquid fuel combustion in BFB has been applied to the analysis of the impact of fluid-dynamic properties of FB (fluidization number, N_f) on the combustion efficiency as well as the influence of the fuel (volatility, water content) to locate the zone of intense burning. For the liquid fuel considered in the numerical experiments an artificial fuel (model-fuel) has been used, which has chemical structure and many physical properties as diesel fuel.

The temperature profiles of modelled FB reactors with combustion of fuel, with and without water content, have been compared to experimental results. The experiments with FB reactors have usually been performed at small-scale facilities [17], and their results after analysis have been scaled up to large-scale boilers. In this paper, the experiments were done on relatively large sized pilot combustion chamber (up to 100 kW) with sunflower oil as the fuel [18]. Therefore, only the parameters for comparison were temperature profiles along the axis of the reactor and mean values of exhaust gases composition.

Numerical simulation of liquid fuels combustion in the FB reactor

The granular flow modeling approach of three-phase BFB comes down to the EE fluidization model that considers gas-particle interaction, taking into account the third liquid phase. The basic EE FB modeling approach considers the gas and FB dense phase (gas-particle system under conditions of the minimum fluidization [19]) as two fluids with different characteristics. The transport equations for momentum transfer of the FB dense phase take into account fluid-particle interactions in conditions of the minimum fluidization velocity, as well as the interaction between the particles themselves. In this case, the third – liquid phase has been included, because of the fuel fed into FB. The interaction between the liquid phase and the gas as well as solid phase have been separately modeled. In the EE approach all phases have the same pressure and that is the pressure of the continuous-primary phase. This model solves the continuity and momentum equations for each phase, and tracks the volume fractions. Further, the additional transport equation for the granular temperature (which represents the solids fluctuating energy) is solved, and the solids bulk and shear viscosity are determined using the kinetic theory of gases on granular flow.

The three phase FB EE granular model governing equations

For modeling the interactions between gas and particle phases, within the suggested EE granular approach to FB modeling, the routines incorporated in the modules of the commercial CFD software package FLUENT 14.0 were used. This code allows presence of several phases within one control volume of the numerical grid, by introducing the volume fraction of each phase. The solid phase represents a granular layer made of spherical particles, with uniform diameters. The mass and momentum conservation equations are solved for each phase separately.

The basic and constitutive equations of the EE granular model of the FB can be described by the following set of expressions [20, 21]:

– continuity equation of the gas phase

$$\frac{\partial}{\partial t}(\alpha_g \rho_g) + \nabla(\alpha_g \rho_g \vec{u}_g) = S_{ev} \tag{1}$$

– continuity equation of the solid phase

$$\frac{\partial}{\partial t}(\alpha_s \rho_s) + \nabla(\alpha_s \rho_s \vec{u}_s) = 0 \tag{2}$$

– continuity equation of the liquid phase

$$\frac{\partial}{\partial t}(\alpha_l \rho_l) + \nabla(\alpha_l \rho_l \vec{u}_l) = -S_{ev} \tag{3}$$

– momentum conservation equation of the gas phase

$$\frac{\partial}{\partial t}(\alpha_g \rho_g \vec{u}_g) + \nabla(\alpha_g \rho_g \vec{u}_g \vec{u}_g) = -\alpha_g \nabla p + \nabla \boldsymbol{\tau}_g + \alpha_g \rho_g \vec{g} + K_{gs}(\vec{u}_g - \vec{u}_s) + K_{gl}(\vec{u}_g - \vec{u}_l) \tag{4}$$

– momentum conservation equation of the solid phase

$$\frac{\partial}{\partial t}(\alpha_s \rho_s \vec{u}_s) + \nabla(\alpha_s \rho_s \vec{u}_s \vec{u}_s) = -\alpha_s \nabla p - \nabla p_s + \nabla \boldsymbol{\tau}_s + \alpha_s \rho_s \vec{g} + K_{gs}(\vec{u}_g - \vec{u}_s) + K_{ls}(\vec{u}_l - \vec{u}_s) \tag{5}$$

– momentum conservation equation of the liquid phase

$$\frac{\partial}{\partial t}(\alpha_l \rho_l \vec{u}_l) + \nabla(\alpha_l \rho_l \vec{u}_l \vec{u}_l) = -\alpha_l \nabla p + \nabla \boldsymbol{\tau}_l + \alpha_l \rho_l \vec{g} + K_{gl}(\vec{u}_g - \vec{u}_l) + K_{sl}(\vec{u}_s - \vec{u}_l) \tag{6}$$

were S_{ev} is the source and sink due to liquid fuel and water evaporation.

The stress tensors of the gas, granular liquid phases can be expressed, respectively:

$$\boldsymbol{\tau}_g = 2\mu_g \mathbf{S}_g + \left(\lambda_g - \frac{2}{3}\mu_g\right)\nabla \vec{u}_g \mathbf{I} \tag{7}$$

$$\boldsymbol{\tau}_s = -p_s \mathbf{I} + 2\alpha_s \mu_s \mathbf{S}_s + \alpha_s \left(\lambda_s - \frac{2}{3}\mu_s\right)\nabla \vec{u}_s \mathbf{I} \tag{8}$$

$$\boldsymbol{\tau}_g = 2\mu_l \mathbf{S}_l + \left(\lambda_l - \frac{2}{3}\mu_l\right)\nabla \vec{u}_l \mathbf{I} \tag{9}$$

where

$\mathbf{S}_k = (1/2)[\nabla \vec{u}_k + (\nabla \vec{u}_k)^T]$, k = g, s, l is the strain rate tensor, $p_s = 2\rho_s \Theta_s (1 + e_s)\alpha_s^2 g_{0s}$ – the pressure of the granular phase [22], while g_{0s} – the radial distribution function, and for Syamlal model it is equal to $g_0(\alpha_s) = 1/1 - \alpha_s + 3\alpha_s/2(1 - \alpha_s)^2$, and e_s is the restitution coefficient.

The viscosity of the granular phase consists of the solids shear viscosity μ_s and the bulk viscosity λ_s. The solids bulk viscosity λ_s is a measure of resistance of solid particles to expansion/compression and according to the Lun *et al.* model [23] is defined as: $\lambda_s = 4/3\alpha_s \rho_s d_s g_{0s}(1 + e_s)(\Theta_s/\pi)^{1/2}$.

The shear viscosity is the result of translator motion (kinetic viscosity $\mu_{s,kin}$), mutual particle collisions (collision viscosity $\mu_{s,coll}$), and frictional viscosity ($\mu_{s,fr}$): $\mu_s = \mu_{s,kin} + \mu_{s,coll} + + \mu_{s,fr}$.

According to the Syamlal model [22], the kinetic viscosity is:

$$\mu_{s,kin} = \frac{\alpha_s d_s \rho_s (\Theta_s \pi)^{1/2}}{12(2-\eta)} \left[1 + \frac{8}{5} \eta(3\eta - 2)\alpha_s g_{0s} \right], \qquad \eta = \frac{1+e_s}{2}, \tag{10}$$

and for the collision viscosity following expression applies: $\mu_{s,coll} = (8/5)\alpha_s \rho_s d_s g_{0s} \eta (\Theta_s/\pi)^{1/2}$. According to the Schaeffer's model [24] frictional viscosity is defined as: $\mu_{s,fr} = (p_s \sin\phi)/2(I_{2D})^{1/2}$, where p_s is the granular phase (solids) pressure, ϕ – the angle of internal friction for the particle, and I_{2D} – the second invariant of the deviator of the strain rate tensor.

The last term of eqs. (4) and (5) is a consequence of the inter-phase interaction drag force, where the coefficient between the fluid and solid (granular) phase, according to the Syamlal and O'Brien model [14], is:

$$K_{gs} = \frac{3\alpha_g \alpha_s \rho_g}{4 u_{r,s}^2 d_s} C_D \left| \vec{u}_s - \vec{u}_g \right|, \quad C_D = \left(0.63 + \frac{4.8}{\sqrt{\mathrm{Re}_s / u_{r,s}}} \right)^2, \quad \mathrm{Re}_s = \frac{\rho_g d_s \left| \vec{u}_s - \vec{u}_g \right|}{\mu_g} \tag{11}$$

The terminal velocity coefficient for the solid phase $u_{r,s}$ was determined as:

$$u_{r,s} = 0.5 \left[A - 0.06\,\mathrm{Re}_s + \sqrt{(0.06\,\mathrm{Re}_s)^2 + 0.12\,\mathrm{Re}_s(2B - A) + A^2} \right] \tag{12}$$

$$A = \alpha_g^{4.14}, \qquad B = \begin{cases} = a\alpha_g^{1.28} & \text{for } \alpha_g \le 0.85 \\ = \alpha_g^{b} & \text{for } \alpha_g > 0.85 \end{cases}$$

The default values of constants *a* and *b* in the coefficient B (eq. 12) are 0.8 and 2.65, respectively. However, despite rigorous mathematical modeling of the associated physics, the drag laws used in the model continue to be semi-empirical in nature. The semi-empirical procedure is proposed primarily for prediction the drag law coefficients that correspond to real minimum fluidization conditions. The constants $a = 0.8$ and $b = 2.65$ in the coefficient B of the Syamlal-O'Brien inter-phase interaction drag force model (eq. 23) are not universal, particularly when it comes to the fluidization regimes with multi-component fluid and in the non-isothermal conditions [15]. For the considered case of combustion in FB it turned out that constants *a* and *b* should have values of 3.2 and 0.6625, respectively [15, 16].

The granular temperature, starting from the equations of conservation of fluctuating granular energy, is:

$$\frac{3}{2}\left[\frac{\partial}{\partial t}(\rho_s \alpha_s \Theta_s) + \nabla(\rho_s \alpha_s \vec{u}_s \Theta_s) \right] = (-\rho_s \mathbf{I} + \boldsymbol{\tau})_s : \nabla \vec{u}_s + \nabla(k_{\Theta s} \nabla \Theta_s) - \gamma_{\Theta s} + \phi_{gs} \tag{13}$$

The diffusion coefficient or conductivity of granular temperature, according to the Syamlal and O'Brain [22], is:

$$k_{\Theta_s} = \frac{15\alpha_s \rho_s d_s \sqrt{\Theta_s \pi}}{4(41 - 33\eta)} \left[1 + \frac{12}{5} \alpha_s g_{0s} \eta^2 (4\eta - 3) \right] \tag{14}$$

The granular energy dissipation due to the inelastic collisions was defined by Lun *et al*. [23]: $\gamma_{\Theta_s} = [12(1 - e_s)g_{0s}/(d_s\sqrt{\pi})]\rho_s\alpha_s\Theta_s^{3/2}$. The exchange of kinetic energy between the phases was determined as: $\phi_{gs} = -3K_{gs}\Theta_s$.

Interphase drag forces due to liquid phase

The momentum conservation equations of the gas phase (4) and solid phase (5) have additional interphase drag force terms, due to presence of liquid phase. Both of these drag force terms: $K_{gl}(\vec{u}_g - \vec{u}_l)$ and $K_{sl}(\vec{u}_s - \vec{u}_l)$, respectively, are also figuring in the momentum conservation equations of the liquid phase (6). For this case the liquid phase has secondary phase characteristics, same as the solid phase. For fluid-fluid flows, each secondary phase is assumed to has form of droplets or bubbles. The exchange coefficient for these types of bubbly, liquid-liquid or gas-liquid mixtures can be written [21]:

$$K_{gl} = \frac{\alpha_g\alpha_l\rho_l f}{\tau_l} \tag{15}$$

where f is the drag function and τ_l, the *particulate relaxation time*, is defined:

$$\tau_l = \frac{\rho_l d_l^2}{18\mu_g} \tag{16}$$

where d_l is the diameter of the bubbles of phase l.

For the simulation of air-liquid interaction the drag function f model of Schiller and Naumann [21] has been used, which is described:

$$f = \frac{C_D\,\mathrm{Re}}{24}$$

$$C_D = \begin{cases} 24\dfrac{1 + 0.15\,\mathrm{Re}^{0.687}}{\mathrm{Re}} & \mathrm{Re} \le 1000 \\ 0.44 & \mathrm{Re} > 1000 \end{cases} \tag{17}$$

The relative Reynolds number for the primary phase g (gas) and secondary phase l (liquid) is obtained:

$$\mathrm{Re}_{qp} = \frac{\rho_g d_l \left|\vec{u}_g - \vec{u}_l\right|}{\mu_g} \tag{18a}$$

The relative Reynolds number for secondary phases l (liquid) and s (solid) is obtained:

$$\mathrm{Re}_{pr} = \frac{\rho_{sl} d_{sl} \left|\vec{u}_s - \vec{u}_l\right|}{\mu_{sl}} \tag{18b}$$

where ρ_{sl} is the mean value of solid and liquid densities, d_{sl} – the mean value of solid particles and liquid droplets, and μ_{sl} – the mixture viscosity of the phases l and s:

$$\mu_{sl} = \alpha_l\mu_l + \alpha_s\mu_s \tag{19}$$

In the present work the inter-phase exchange coefficient between liquid and solid phase is obtained by Gidaspow *et al.* drag model [25]. It is combination of Wen and Yu model and the Ergun equation [21].

When $\alpha_l > 0.8$, the fluid-solid exchange coefficient K_{sl} has the following form:

$$K_{\mathrm{sl}} = \frac{3}{4} C_{\mathrm{D}} \frac{\alpha_{\mathrm{s}} \alpha_{\mathrm{l}} \rho_{\mathrm{l}} \left| \vec{\mathrm{u}}_{\mathrm{s}} - \vec{\mathrm{u}}_{\mathrm{l}} \right|}{d_{\mathrm{s}}} \alpha_{\mathrm{l}}^{-2.65} \text{ where } C_{\mathrm{D}} = \frac{24}{\alpha_{\mathrm{l}} \mathrm{Re}_{\mathrm{s}}} [1 + 0.15(\alpha_{\mathrm{l}} \mathrm{Re}_{\mathrm{s}})^{0.687}] \quad (20)$$

When $\alpha_l \leq 0.8$ than the expression can be used:

$$K_{\mathrm{sl}} = 150 \frac{\alpha_{\mathrm{s}}(1 - \alpha_{\mathrm{l}})\mu_{\mathrm{l}}}{\alpha_{\mathrm{l}} d_{\mathrm{s}}^2} + 1.75 \frac{\rho_{\mathrm{l}} \alpha_{\mathrm{s}} \left| \vec{\mathrm{u}}_{\mathrm{s}} - \vec{\mathrm{u}}_{\mathrm{l}} \right|}{d_{\mathrm{s}}} \quad (21)$$

Equations for energy and conservation of chemical components

The proposed model includes the energy equations and the transport equations of chemical species conservation with the source terms due to the conversion of chemical components, which are presented by eqs. (22)-(25):

– energy equation of gas phase

$$\frac{\partial}{\partial t}(\alpha_{\mathrm{g}} \rho_{\mathrm{g}} c_{p,\mathrm{g}} T_{\mathrm{g}}) + \nabla(\alpha_{\mathrm{g}} \rho_{\mathrm{g}} \vec{\mathrm{u}}_{\mathrm{g}} c_{p,\mathrm{g}} T_{\mathrm{g}}) =$$

$$= \nabla\left(\frac{k_{\mathrm{g}}}{c_{p,\mathrm{g}}} \nabla T_{\mathrm{g}}\right) + \nabla\left(\sum_i \alpha_{\mathrm{g}} \rho_{\mathrm{g}} D_{i,\mathrm{m}} c_{p,i} T_{\mathrm{g}} \nabla Y_{\mathrm{i}}\right) + \Sigma H_{r,\mathrm{l}} - h_{\mathrm{sg}}(T_{\mathrm{s}} - T_{\mathrm{g}}) - h_{\mathrm{gl}}(T_{\mathrm{g}} - T_{\mathrm{l}}) \quad (22)$$

– energy equation of solid phase

$$\frac{\partial}{\partial t}(\alpha_{\mathrm{s}} \rho_{\mathrm{s}} c_{p,\mathrm{s}} T_{\mathrm{s}}) + \nabla(\alpha_{\mathrm{s}} \rho_{\mathrm{s}} \vec{\mathrm{u}}_{\mathrm{s}} c_{p,\mathrm{s}} T_{\mathrm{s}}) = \nabla\left(\frac{k_{\mathrm{s}}}{c_{p,\mathrm{s}}} \nabla T_{\mathrm{s}}\right) + h_{\mathrm{sg}}(T_{\mathrm{s}} - T_{\mathrm{g}}) + h_{\mathrm{sl}}(T_{\mathrm{s}} - T_{\mathrm{l}}) \quad (23)$$

– energy equation of liquid phase

$$\frac{\partial}{\partial t}(\alpha_{\mathrm{l}} \rho_{\mathrm{l}} c_{p,\mathrm{l}} T_{\mathrm{l}}) + \nabla(\alpha_{\mathrm{l}} \rho_{\mathrm{l}} \vec{\mathrm{u}}_{\mathrm{l}} c_{p,\mathrm{l}} T_{\mathrm{l}}) = \nabla\left(\frac{k_{\mathrm{l}}}{c_{p,\mathrm{l}}} \nabla T_{\mathrm{l}}\right) +$$

$$+ \nabla\left(\sum_i \alpha_{\mathrm{l}} \rho_{\mathrm{l}} D_{i,m} c_{p,\mathrm{i}} T_{\mathrm{l}} \nabla Y_{\mathrm{i}}\right) - h_{\mathrm{sl}}(T_{\mathrm{s}} - T_{\mathrm{l}}) + h_{\mathrm{gl}}(T_{\mathrm{g}} - T_{\mathrm{l}}) \quad (24)$$

– conservation equations for chemical components

$$\frac{\partial}{\partial t}(\alpha_k \rho_k Y_i) + \nabla(\alpha_k \rho_k \vec{\mathrm{u}}_k Y_i) = \nabla(\alpha_k \rho_k D_{i,m} \nabla Y_i) + R_i, \qquad k = \mathrm{g}, \mathrm{l} \quad (25)$$

The energy balance equations for all three phases are connected through the interphase volumetric heat transfer coefficient (h), which has given by Gunn [26] for gas-solid and liquid-solid interphase heat transfer. For the gas-liquid interphase volumetric heat transfer coefficient (h_{gl}) the formulation of Ranz and Marshall [27, 28] has been used. The granular conductivity coefficient, for conditions of the developed fluidization, has very high values ($\approx$100 $\mathrm{Wm^{-1}K^{-1}}$) [19]. The radiation heat transfer is not included in this stage of the model developing. This assumption may be valid if it is taken into account that the convective heat transfer and conduction in BFB are very intensive [19].

Combustion model

The source term R_i in set of eqs. (24) corresponds to the chemical conversion rates of the components i. The chemical reactions, used for combustion model within presented numerical procedure for liquid fuels combustion in FB, are homogeneous and heterogeneous. The homogeneous reactions are: first step combustion of the evaporated fuel (to CO and H_2O) and CO oxidation; while heterogeneous reactions are liquid fuel evaporation, the direct first step of the liquid fuel combustion and the water evaporation (when fuel comprises water).

The production and conversion of species i due to the chemical reactions enter as a source/sink term R_i in the transport equations of chemical species:

$$R_i = M_i \sum_{l=1}^{N_R} (\nu_{il}'' - \nu_{il}') k_l \left(\prod_{\text{educts}} c^{\nu_{il}'} - \frac{1}{K_c} \prod_{\text{products}} c^{\nu_{il}''} \right) \tag{26}$$

where N_R is the number of reactions l. For each of chemical reactions l the balance of atom species A_l must be satisfied:

$$\sum_{i=1}^{N_S} \nu_{il}' A_i = \sum_{i=1}^{N_S} \nu_{il}'' A_i \tag{27}$$

The laminar final rate reactions have been assumed for all homogeneous combustion processes, and for the heterogeneous reaction of direct first step fuel combustion, thus the reaction rate constants k_l are determined by the Arrhenius expression:

$$k_l = k_{o,l} T^a \exp\left(-\frac{E_{a,l}}{\mathrm{R}T} \right) \tag{28}$$

Fuel and water vaporization model

The reaction rate constants k_i for the fuel and water vaporization reactions has to be separately modeled. The mathematical modeling of the evaporation of the liquid fuel fed in fluidized furnace had to be differently considered, if the temperature of fuel is higher or lower than the boiling point of the fuel ($T_l \geq T_{bp}$, $T_l < T_{bp}$).

In [29] an analysis of the prediction of the discrete phase droplet convective boiling can be found. The analysis is done for the case that the temperature of the droplet has reached the boiling temperature, T_{bp}. However, the here considered case, based on a continuous introduction of liquid fuel into the hot FB, significantly differs from the discrete phase droplet convective boiling. Because of that, somewhat changed equation for heat balance of the liquid fuel fed into the heated FB is used:

$$(1 - Y_{H_2O}) \dot{m}_{fu} c_{p,fu} (T_{bp} - T_o) + \dot{m}_p q_{lat} = h_{fb} S_l (T_{fb} - T_{bp}) + Q_{rad} \tag{29}$$

where $\dot{m}_{fu}$ and $\dot{m}_p$ are the mass flows of fuel (with water if it is included), and vapor, respectively, Y_{H_2O} – the mass fraction of water in the fuel, T_o and T_{fb} – the temperatures of inlet fuel and FB temperature, respectively, q_{lat} – the latent heat, and Q_{rad} – the radiation heat transfer.

It is assumed that the fuel temperature cannot be higher than the boiling point of the fuel. The radiation term can be neglected due to the high values of convective heat transfer, h_{fb}, and the expression for the rate of evaporation can be written:

$$\dot{m}_p = \frac{(1 - Y_{H_2O}) \dot{m}_{fu} c_{p,fu} (T_{bp} - T_o) + h_{fb} S_l (T_{fb} - T_{bp})}{q_{lat}} \tag{30}$$

The expression for the rate of water evaporation when the fuel temperature is equal to boiling point can be written in the same manner:

$$\dot{m}_{p,\mathrm{H_2O}} = \frac{Y_{\mathrm{H_2O}}\dot{m}_{\mathrm{fu}}c_{p,\mathrm{fu}}(T_{\mathrm{bp,H_2O}} - T_o) + h_{\mathrm{fb}}S_{\mathrm{l}}(T_{\mathrm{fb}} - T_{\mathrm{bp,H_2O}})}{q_{\mathrm{lat,H_2O}}} \tag{31}$$

Therefore, the reaction rate constants for the fuel and water vaporization reactions can be expressed as $k_p = \dot{m}_p / V_{\mathrm{l}}$, where V_{l} is the liquid phase volume. In the presented model the value of the liquid phase surface and volume have been numerically determined by an in-house-developed subroutine.

In case that the fuel temperature is lower than the boiling point ($T_{\mathrm{l}} < T_{\mathrm{bp}}$) the kinetic rate, k_i, was defined by input of an Arrhenius type pre-exponential factor and an activation energy, eq. (28).

Numerical procedure

Numerical solving of the governing equations of the FLUENT EE granular model, eqs. (1)-(6), (22)-(25), is performed by the method of control volumes whereby the coupling and correction of the velocity and pressure is carried out for multiphase flows with the phase coupled SIMPLE (PCSIMPLE) algorithm. The discretisation of the convective terms was carried out with the second-order upwind scheme.

The calculations were non-stationary, with a time step of 1 ms, which allowed a relatively quick convergence with a maximum of 100 iterations per time step, whereby the convergence criterion between two iterations was set to $1 \cdot 10^{-3}$. The number of time steps, *i. e.* the total simulation time, has been determined by the time required for the fluid to pass through the entire reactor space. The computational domain consists of the zones: layer of particles in the FB and the free flow above the FB. The entire numerical grid consists of more than 10000 nodes (fig. 1.).

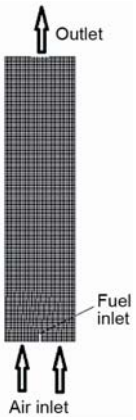

Figure 1. Schematic view of the geometry of numerically simulated fluidization reactor

The inter-phase interaction drag force model eqs. (11)-(12), (15)-(21) as well as equations for the reaction rate constants (30), (31) for the fuel and water vaporization reactions, were included in the numerical simulation process by the specialized subroutines in the C programming language (*user defined functions*), wherewith the user is able to upgrade individual parts of the core Fluent's code.

The proposed calculation procedure is performed through two steps: (1) the calculation of transformation of the fixed granular bed to the fully developed bubble fluidization (sections *The three phase fludized bed Euler-Euler granular model governing equations* and *Equations for energy and conservation of chemical components*), for desired hydrodynamic conditions; (2) continuing the calculation procedure with including the combustion model (sections *Combustion model*). The matrix values of the variables calculated in the first computing step were used as the initial conditions for the second step of the calculating process. Moreover, in the second step the boundary conditions are changed introducing the inlet fuel flow and the equations of chemical species with the source terms due to chemical reactions were activated. The calculation process is ended when the quasi-stationary conditions are reached, *i. e.* when the mean values of calculated thermophysical properties are changed within the constant range.

All cases of numerical simulation of the processes in a fluidized combustion chamber was performed on the fluidization reactor with height of 2.3 m and width of 0.4 m, as it is shown in the schematic view of the reactor. The modeled granular bed consists of particles with the diameter of 0.8 mm and density of 2600 kg/m^3, where the height of the bed in the bulk condition is 0.3 m. The fuel was entering through the vertical nozzle placed axially on the bottom of the reactor (fig. 1). Height of the nozzle for the fuel introduction is 0.05 m. Air for fluidization was introducing annularly as is shown in fig. 1. The inlet temperature of the air and fuel was ambient (300 K).

The results of the first step of the presented numerical simulation are presented in fig. 2, which shows the solid volume fraction distribution during the bubbled fluidization development period. The first step of presented numerical simulations are performed by numerical simulation of the bubbled fluidization development of sand particles fluidized with air which ensures the fluidization number $N_f \approx 3$ on temperature of 1200 K.

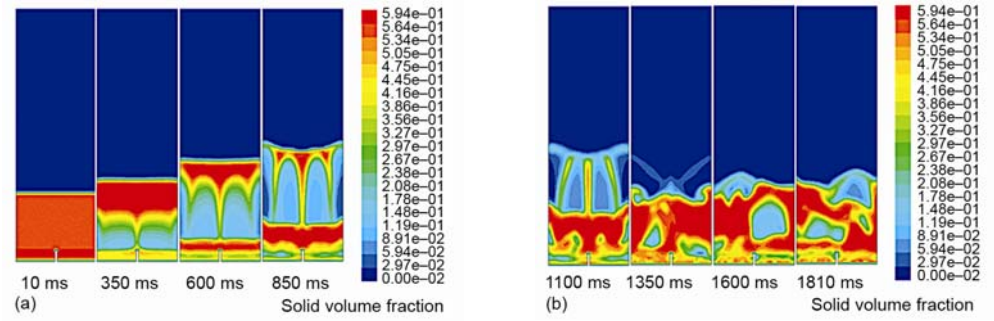

Figure 2. Development of the solid volume fraction distribution within the fluidized reactor before the combustion is started

Calculated gas temperature distributions the result of the second step numerical simulation of diesel fuel combustion in FB with specified conditions without moisture are shown in fig. 3. The inlet mass flow rate of the air and pure diesel fuel was 0.11627 kg/s and 0.002586 kg/s, respectively, which corresponds to the excess air ratio of $\lambda = 3$. Gas temperature distributions shown in fig. 3. represents the thermal conditions within fluidized reactor for the period starting from 5 to 8 seconds after the fuel introduction into the heated FB. The temperature field in the zone of intense reaction in fluidized combustion chamber stochastically changes in time but within a constant temperature range (fig. 3), so a quasi-stationary processes can be assumed in that type of FB combustion.

Experiments with combustion of the jet-fed fuel into the FB

Trial experiments with combustion in the fluidization furnace were done on a pilot-facility, shown schematically in fig. 4. The experimental installation has been dimensioned, designed, and built in a way that the results obtained during investigations on it can be used as design parameters for the construction of real-scale facilities for combustion of solid or liquid fuel. The combustion chamber has a rectangular cross-section of 0.295 × 0.290 m and height of 2.3 m. The power of the experimental chamber is up to 100 kW.

In the analyzed case the fuel (sunflower oil) was fed into the FB at the angle of 38^o, and it was possible to regulate the distance of the nozzle outlet from the bed bottom. The fuel is

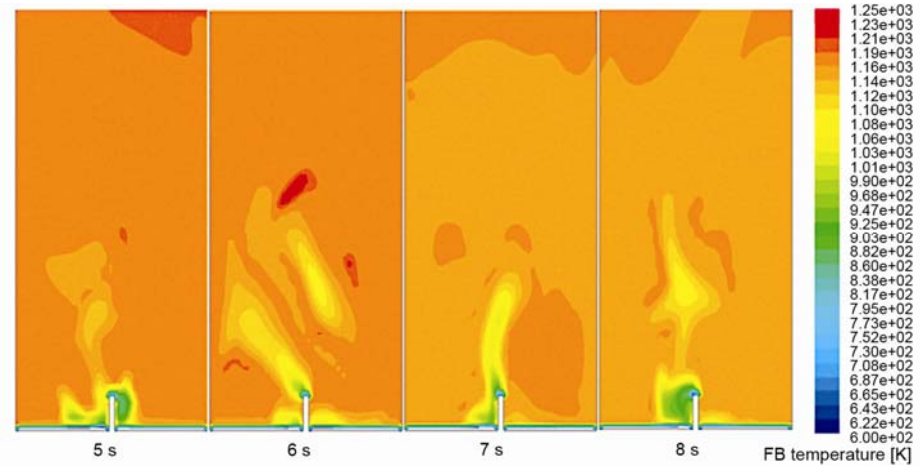

Figure 3. The change in time of the quasi-stationary temperature field in the fluidized combustion chamber

introduced into the experimental facility with the fuel feeding system (7) through the tubular nozzle (17). The FB inert material consisted of quartz sand particles with medium diameter of 0.8 mm, deposited density of 1310 kg/m^3, and the height of 0.323 m. The fluidization gas was air. The air is supplied to the FB through the distributor (4). The flue gases from the particles burn out in the furnace space above the bed.

During the stationary regime of the furnace operation, temperatures inside the FB and concentrations of the combustion products were monitored continuously. Figure 4 shows temperature measuring points along the vertical center line of the reactor (marked as $T_1 - T_7$).

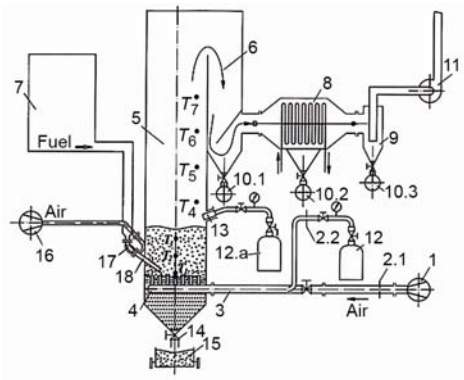

Figure 4. Scheme of the experimental facility with the liquid fuel feeding system

Experiments were conducted with the model fuel – cooking oil, which has no mechanical or other impurities and has lower viscosity than real industrial waste liquid fuels [18]. Realistic conditions were simulated by adding water to the model fuel. The stationary regimes of combustion of model fuel were followed, for different depths of nozzle in the FB and for different compositions of the model fuel, by adding water to oil (tab. 1).

In all investigated regimes, stable combustion conditions were achieved, with average bed temperature of 850-900 °C, which would stabilize soon after the start. Very favorable emissions were achieved, with very low CO emissions.

Comparison between numerical simulation and experimental results

In the experiments with a pilot furnace with liquid fuel feeding into the FB (described in the section *Experimentas with combustion of the jet-fed fuel into the FB*), withdrawal of the intense combustion zone has been observed towards the areas below the bed

Table 1. Operating parameters of experimental FB furnace

Regime	Fuel flow rate [kgh^{-1}]	Temperature of the active part of the FB [°C]				Gas composition						λ	Air flow rate [kgh^{-1}]
		T_2	T_3	T_4	T_5	CO_2	O_2	CO	SO_2	NO	NO_2		
						%		ppm					
Fuel without water	4.08	663.3	898.3	899.2	904.9	5.1	14.95	16.18	0,0	12,18	0,0	2.95	142.7
Fuel with 20 mass % of water	4.32	645.8	870.7	870.8	883.6	4,73	15,32	2.08	0,0	10,37	0,0	3.	142.2

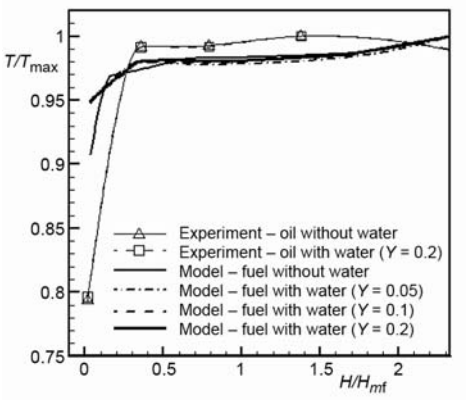

Figure 5. Normalized temperature profiles along fluidized combustor height numerically and experimentally obtained

surface during the combustion of liquid fuels without water content and also in case with significant water content [18]. Very similar phenomena has been shown during numerous numerical experiments (which procedure has been described in the section *Numerical procedure*) with combustion of test-fuel ($C_{10}H_{22}$) in 2-D fluidized reactor. As it can be observed in fig. 5. temperature profiles along central vertical line of the FB combustor obtained by measurements as well as by calculation show that very high temperatures can be achieved on relatively low heights of the reactor. In other words, both experiments and numerical simulations show that in considered FB combustor the intense combustion zones have been withdrawn deep into the FB. This is very convenient, because in this way provides efficient and complete combustion within a relatively small volume.

The ordinate in the diagram of fig. 5 (as well as in fig. 6 and 7) represents a dimensionless temperature, *i. e.* ratio of given temperature, and maximum temperature (theoretical combustion temperature) in given conditions. Thereby, it should be noted that the axial temperature profile, obtained by the model, have been formed by averaging of the temperatures at cross-sections at the considered heights of the reactor. Also on presented diagrams the abscissa represents the dimensionless height of the furnace, which is defined as ratio between the height of the reactor and the height of the fixed bed (h_{fb}).

Figure 5 also shows the results of physical and numerical experiments with combustion of fuel with and without water content. Considered type of fluidizing combustion chamber is of particular importance for use in combustion of unconventional fuels that often contain water in a substantial amount, so the exposed analysis is of significance. As it is shown in fig. 5, the water content in the fuel has small impact on temperature profiles along the axis of the reactor as shown by the experiments and numerical simulation. It can be observed even slightly higher relative temperatures in the bottom of the FB for the cases of combustion of the fuels that contain water. This phenomenon is more pronounced in results of the numerical

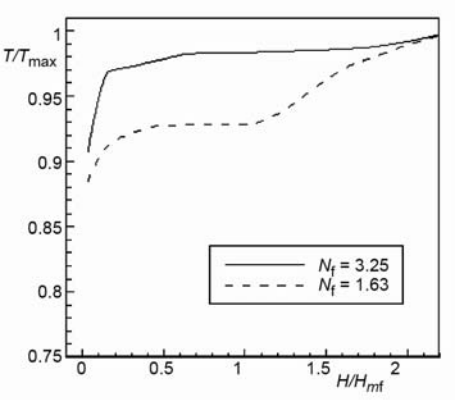

Figure 6. Calculated temperature profiles along fluidized combustor height at conditions of different fluidization number (N_f)

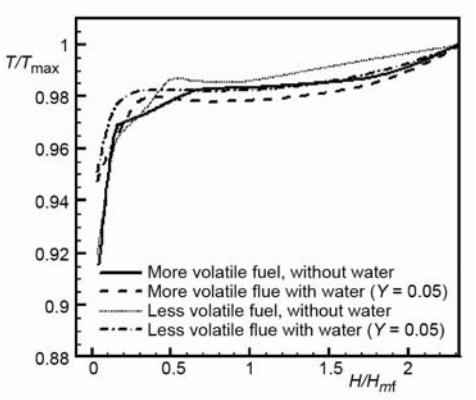

Figure 7. Modeled temperature profiles along fluidized combustor height for combustion of more and less volatile fuel

simulations. It can be concluded that the water content in the fuel affects to some degree the withdrawal of the intense combustion zone in FB furnace towards the lower zones. This also points to the fact that in the regimes with fuel that contains water the combustion position is slightly lower, *i. e.* that little more efficient combustion is achieved. The noted effect can be explained by the expansion of the steam what contributes to getting the favorable (stoichiometric and over-stoichiometric) mixtures of fuel and oxidizer. According to the present model of heterogeneous combustion of liquid fuels in FB (section *Fuel and water vaporization model*) the surface area between the liquid phase and FB greatly affects the combustion rate, eq. (30), and since sudden expansion of the water vapor is causing an increase of the liquid phase, it may be assumed that presence of water in the fuel can influence the increase of the heterogeneous combustion rate.

In the diagram of the experimental results (fig. 5), a slight decline in temperature over the FB can be seen, as a consequence of non-ideal insulation of the experimental reactor.

The presented method of numerical simulation of combustion in a bubbling FB can be used for the purposes of analyzing the impact of hydrodynamic characteristics of BFB on the properties and efficiency of liquid fuel combustion in these reactors. The diagrams in fig. 6 show the numerical and experimental results of comparing the liquid fuel combustion in FB with different N_f. The N_f is the ratio between of the fluidization gas velocity and the minimum fluidization velocity and represents a measure of the mixing intensity in FB. As seen in fig. 6, the fuel combustion in FB at conditions of higher FB mixing rate allows complete combustion in the lower zones of the reactor, while in the case of the combustion at lower N_f, major part of the combustion process takes place above the bed. As it is already mentioned, the progress of the combustion process within the lower zone of the FB is desirable from the standpoint of energy efficiency as well as environmental reasons.

For the organization of combustion of liquid fuels in a FB it is important to consider the impact of fuel volatility on the combustion characteristics. This is the reason for presenting the results of numerical experiments with burning the same fuel type and in the same conditions but with different volatility (fig. 7). As already noted, the test fuel with thermophysical properties as a diesel fuel was used in numerical experiments (described in Chapter *Combustion model*). This fuel devolatilize according to the model eq. (30), and the evaporated

fuel combust according to a two-step combustion model as a finite rate reaction, while at the same time part of the liquid fuel is directly subjected to the first step of combustion (to CO), as it is shown in tab. 2. Numerical experiments have been done in two cases: with fuels that have more and less pronounced volatility characteristics (tab. 2).

Table 2. Modeled heterogeneous reactions of liquid fuel combustion in the FB

Reaction		Pre-exponential factor k_o	Activation energy E_a [Jkmol^{-1}]	Order reaction of the first reactant	Order reaction of the second reactant
Volatility	Formula				
More	$C_{10}H_{22\ (liquid)} \rightarrow C_{10}H_{22\ (vapour)}$	eq. (30)		1	-
	$C_{10}H_{22(liquid)} + 10.5O_2 = 10CO + 11H_2O$	2.59E+12	2.26E+08	0.25	1.5
Less	$C_{10}H_{22\ (liquid)} \rightarrow C_{10}H_{22\ (vapour)}$	eq. (30) multiplied by 0.5		1	-
	$C_{10}H_{22(liquid)} + 10.5O_2 = 10CO + 11H_2O$	5.59E+12	2.16E+08	0.25	1.5

Figure 7 shows the results of numerical simulation of combustion in FB of liquid fuels, with and without water that have more and less pronounced volatility characteristics. As seen in fig. 7, in both cases, when significant part of the intensive combustion zone is located within the area of FB. However, somewhat higher normalized temperatures in the lower zones of the FB are achieved with fuel which is less volatile. This is because in case of less volatile fuel combustion most of the reactions take place in the lower zones of the bed and there is a less possibility of the unburned fuel vapor passing by bubbles in higher zones of the reactor. The same effect is observed also in the simulation of combustion of fuel containing water (fig. 7), whereby previously discussed impact of the water presence in the fuel also can be seen – the more intensive combustion zone is slightly pulled back to the lower areas of the FB.

Conclusions

A comprehensive numerical model of the liquid fuels combustion in a 2-D bubbled FB is proposed. The developed numerical model of the fluidization is based on the Eulerian-Eulerian granular flow simulation method including the kinetic theory of granular flow for the particles motion modeling. In the standard Eulerian-Eulerian granular model the third phase has been included as a liquid phase due to fuel which has been fed into FB.

The interaction between the liquid phase and the gas, as well as solid phase, has been separately modeled. For the inter-phase interaction drag force definition the model by Syamlal and O'Brien [14] has been used, wherein the constants *a* and *b* of the model coefficient B eq. (23) have values of 3.2 and 0.6625, respectively. For the simulation of air-liquid interaction the drag function *f* model of Schiller and Naumann has been used. The inter-phase exchange coefficient between liquid and solid phase is obtained by Gidaspow [25] drag model.

The proposed model includes the energy equations and the transport equations of chemical species conservation with the source terms due to the conversion of chemical components. The chemical reactions, used for combustion model within presented numerical procedure for liquid fuels combustion in FB, are homogeneous and heterogeneous. It is assumed that part of the liquid fuel evaporates and then the steam burns according to the two-step

combustion concept while part of the fuel is burned directly. The in-house developed evaporation model is based on mass-heat balance between the input fuel enthalpy, the latent heat of evaporation and heat transfer between FB and liquid phases.

The numerical procedure consists of two steps. In the first step of the calculation, the transformation of the fixed granular bed to fully developed bubble fluidization for desired hydrodynamic conditions is performed. In the second step, the boundary conditions are changed by introducing the inlet fuel flow; and the equations of chemical species with the source terms due to chemical reactions were activated.

Trial experiments with the liquid fuel combustion in the fluidization furnace were done on a pilot-facility with power up to 100 kW. Two stationary regimes of combustion of model fuel were followed for different regimes: fuel without and with water.

The general conclusion of the results of experiments and numerical simulations is that in the normalized temperature profiles along the FB combustor, very high temperatures on relatively low heights of the reactor were achieved. This leads to the conclusion that in considered FB combustor the intense combustion zones have been withdrawn deep into the FB, which means that almost the entire combustion processes has been completed within the fluidization gas-particle zone. Similar temperature profiles with high temperatures deep in the FB were also obtained in combustion of liquid fuels containing admixtures of water. However, slightly higher normalized temperatures in the bottom of the FB are observed for the cases of the fuels containing water combustion. This phenomenon is more pronounced in results of the numerical simulations.

The liquid fuel combustion in FB at conditions of larger N_f (3.25) enables almost complete combustion in the lower zones of the reactor, while in the case of the combustion at lower N_f (1.63) major part of the combustion process takes place above the FB.

The results of numerical simulation of combustion in FB of liquid fuels with and without water that have more and less pronounced volatility characteristics are presented. In both cases when less and more volatile fuel combust, significant part of the intensive combustion zone is located within the area of FB, but somewhat higher normalized temperatures in the lower zones of the FB are achieved with the less volatile fuel.

Acknowledgment

The authors wish to thank the Serbian Ministry of Education, Science and Technological Development for financing the project *Improvement of the industrial fluidized bed facility, in scope of technology for energy efficient and environmentally feasible combustion of various waste materials in fluidized bed* (Project TR33042).

Nomenclature

C_D – drag coefficient, [–]
c_p – specific heat, [Jkg^{-1}K^{-1}]
c – molar concentration, [kmolm^{-3}]
$D_{i,m}$ – mass diffusion coefficient for species i, [m^{2}s^{-1}]
d_p, d_s – particle mean diameter, [m]
E_a – activation energy, [Jmol^{-3}]
e_s – restitution coefficient, [–]
$\bar{g}$ – gravity acceleration, [ms^{-2}]
g_{0s} – radial distribution function, [–]
H – height, [m]
H_e – heating value of reaction h, [Jkg^{-1}]
H_{fb} – height of the fixed bed, [m]
H_l – heating value of reaction l, [Jkg^{-1}]
h – heat transfer coefficient with specific surface, [Wm^{-2}K^{-1}]
I – unity matrix, [–]
$\mathbf{I}_{2D}$ – second invariant of deviator of the strain rate tensor, [–]
K_c – reaction equilibrium constant, [–]
K_{gs} – gas/solid momentum exchange, [kgs^{-1}]
k_t – thermal conductivity, [Wm^{-1}K^{-1}]
k_o – pre-exponential coefficient, [s^{-1}]

$k_{\Theta s}$ – diffusion coefficient for granular energy, [kgm^{-1}K^{-1}]
l – liquid, number of reaction, [–]
N_f – fluidization number, [–]
p – pressure, [Pa]
R – universal gas constant, [Jmol^{-1}K^{-1}]
$\mathbf{S}_k$ – strain rate tensor, [–]
T – absolute temperature, [K]
T_{max} – maximal temperature in the regime, [K]
$\vec{u}$ – instantaneous velocity vector, [ms^{-1}]
Y_i – species mass fraction, [–]
Y_{H_2O} – water mass fraction in the fuel, [–]

Greek symbols

α – phase void fraction, [–]
$\gamma_{\Theta s}$ – collisional dissipation energy, [kgs^{-3}m]
Θ_s – granular temperature, [kgm^{-2}s^{-2}]
λ – bulk viscosity, [kgm^{-1}s^{-1}]
$\mu_{s,coll}$ – collisional viscosity, [kgm^{-1}s^{-1}]
$\mu_{s,fr}$ – frictional viscosity, [kgm^{-1}s^{-1}]
$\mu_{s,kin}$ – kinetic viscosity, [kgm^{-1}s^{-1}]
ν – stoichiometric number, mole number, [–]
ρ – density, [kgm^{-3}]
$\boldsymbol{\tau}$ – phase stress-strain tensor, [Pa]
ϕ – angle of internal friction for the particle, [°]
ϕ_{gs} – transfer rate of kinetic energy, [Js^{-1}]

Subscripts

b – fluidized bed
fu – fuel
g – gas
l – liquid
s – solid

References

[1] Tsuji, Y., *et al.*, Discrete Particle Simulation of Two Dimensional Fluidized Bed. *Powder Technology, 77* (1993), 1, pp. 79-87
[2] Hoomans, B. P. B., *et al.*, Discrete Particle Simulation of Bubbling and Slug Formation in a Two-Dimensional Gas– Fluidized Bed: A Hard-Sphere Approach. *Chemical Engineering Science, 51* (1996), 1, pp. 99-118
[3] Gera, D., *et al.*, Computer Simulation of Bubbles in Large-Particle Fluidized Beds, *Powder Technol*, *98* (1998), 1, pp. 38-47
[4] Ibsen, C., *et al.*, Comparison of Multifluid and Discrete Particle Modelling in Numerical Predictions of Gas Particle Flow in Circulating Fluidised Beds, *Powder Technol*, *149* (2004), 1, pp. 29-41
[5] Bokkers, G. A., *et al.*, Mixing and Segregation in a Disperse Gas-solid Fluidised Bed: A Numerical and Experimental Study, *Powder Technol.*, *140* (2004), 3, pp. 176-186
[6] Di Renzo, A., Di Maio, F. P., Homogeneous and Bubbling Fluidization Regimes in DEM–CFD Simulations: Hydrodynamic Stability of Gas and Liquid Fluidized Beds, *Chem. Eng. Sci*., 62 (2007), 1-2, pp. 116-130
[7] Enwald, H., *et al.*, Simulation of the Fluid Dynamics of a Bubbling Fluidized Bed. Experimental Validation of the Two-Fluid Model and Evaluation of a Parallel Multiblock Solver, *Chem. Eng. Sci*., *54* (1999), 3, pp. 311-328
[8] Cammarata, L., *et al.*, 2D and 3D CFD Simulations of Bubbling Fluidized Beds Using Eulerian–Eulerian Models, *Int. J. Chem. Reactor Eng., 48* (2003), 1, pp. 1-10
[9] Behjat, Y., *et al.*, CFD Modeling of Hydrodynamic and Heat Transfer in Fluidized Bed Reactors*, Int. Commun Heat Mass Transfer*, *35* (2008), 3, pp. 357-368
[10] Gidaspowa, D., *Multiphase Flow and Fluidization: Continuum and Kinetic Theory Descriptions*, Academic Press, San Diego, Cal., USA, 1994
[11] Van Wachem, B. G. M., *et al.*, Comparative Analysis of CFD Models of Dense Gas-Solid Systems. *Aiche Journal, 47* (2001), 5, pp. 1035-1051
[12] Van Der Hoef, M. A., *et al.*, Computational Fluid Dynamics for Dense Gas-Solid Fluidized Beds: A Multi-Scale Modeling Strategy. *Chemical Engineering Science, 59* (2004), 22. pp. 5157-5165
[13] Chapman, S., Cowling, T. G., *The Mathematical Theory of Non-Uniform Gases*. 3rd edition, Cambridge University Press, Cambridge, UK, 1970
[14] Syamlal, M., O'Brien, T. J., Simulation of Granular Layer Inversion in Liquid Fluidized Beds, *Int. J. Multiphase Flow*. *14* (1988), 4, pp. 473-481
[15] Nemoda, S., Đ., *et al.*, Euler-Euler Granular Flow Model of Liquid Fuels Combustion in a Fluidized Reactor, *J. Serb. Chem. Soc. 80* (2015), 3, pp. 377-389
[16] Nemoda, S. Đ., *et al.*, Euler-Euler Granular Flow Model Applied on Numerical Simulation of Liquid Fuels Combustion in a Fluidized Bed, *Proceedings on CD ROM,* 16th Symposium on Thermal Science and Engineering of Serbia, Sokobanja, Serbia, 2013, pp. 311-323.

[17] Wojciech, P., *et al.*, Modeling of Particle Transport and Combustion Phenomena in a Large-Scale Circulating Fluidized Bed Boiler Using a Hybrid Euler–Lagrange Approach. *Particuology, 16* (2014), Complete, pp. 29-40
[18] Mladenović, M. R., *et al.*, Vertical Temperature Profile in the Installation for the Combustion of Waste Fuels in the Fluidized Bed Furnace, *Proceedings on CD-ROM,* 15th Symposium on Thermal Science and Engineering of Serbia, Sokobanja, Serbia, 2011, pp 490-499
[19] Oka, S., *Fluidized Bed Combustion*, Marcel Decker Inc., New York, USA, 2004
[20] Vejahati, F., *et al.*, CFD Simulation of Gas-solid Bubbling Fluidized Bed: A New Method for Adjusting Drag Law, *Can. J. Chem. Eng., 87* (2009), 1, pp. 19-30
[21] Shailendra Kr. Pandey, *CFD Simulation of Hydrodynamics of Three Phase Fluidized Bed,* M. Sc. thesis, National Institute of Technology, Orissa, India, 2010
[22] Syamlal, M. W. R., O'Brien, T. J., *MFIX Documentation Theory Guide*, U.S. Department of Energy Office of Fossil Energy Morgantown Energy Technology Center, Morgantown. W. Va., USA, 1993
[23] Lun, C. K. K., *et al.*, Kinetic Theories for Granular Flow: Inelastic Particles in Couette Flow and Slightly Inelastic Particles in a General Flow Field, *J. Fluid Mech., 140* (1984), Mar., pp. 223-256
[24] Schaeffer, D. G., Instability in the Evolution Equations Describing Incompressible Granular Flow, *J. Diff. Eq.*, *66* (1987), 1, pp. 19-50
[25] Gidaspow, D., *et al.*, Hydrodynamics of Circulating Fluidized Beds. Kinetic Theory Approach, Fluidization VII*, Proceedings,* 7th Engineering Foundation Conference on Fluidization*,* Brisbane, Australia, 1992, pp. 75-82
[26] Gunn, D. J., Transfer of Heat or Mass to Particles in Fixed and Fluidized Beds, *Int. J. Heat Mass Transfer, 21* (1978), 4, pp. 467-476
[27] Ranz, W. E., Marshall, W. R. Jr., Evaporation From Drops. Part I. *Chem. Eng. Prog., 48* (1952), 3, pp. 141-146
[28] Ranz, W. E., Marshall, W. R. Jr., Evaporation From Drops. Part II. *Chem. Eng. Prog*., *48* (1952), 4, pp. 173-180
[29] Kuo, K. K. Y., *Principles of Combustion*, John Wiley and Sons, New York, USA, 1986

Paper submitted: October 25, 2015
Paper revised: November 4, 2015
Paper accepted: November 5, 2015